Phononic crystals in superfluid thin-film helium

Korsch, Alexander Rolf; Fiaschi, Niccolò; Gröblacher, Simon

DOI
10.1103/PhysRevApplied.22.L041005

Publication date
2024

Document Version
Final published version

Published in
Physical Review Applied

Letter

Phononic crystals in superfluid thin-film helium

Alexander Rolf Korsch,[1,2,3] Niccolò Fiaschi,[3] and Simon Gröblacher[3,*]

[1] *Department of Physics, Fudan University, Shanghai 200433, People's Republic of China*

[2] *Department of Physics, School of Science, Westlake University, Hangzhou 310030, People's Republic of China*

[3] *Kavli Institute of Nanoscience, Department of Quantum Nanoscience, Delft University of Technology, 2628CJ Delft, Netherlands*

(Received 28 February 2024; revised 26 September 2024; accepted 1 October 2024; published 18 October 2024)

In recent years, nanomechanical oscillators in thin films of superfluid helium have attracted attention in the field of optomechanics due to their exceptionally low mechanical dissipation and optical scattering. Mechanical excitations in superfluid thin films—so-called third sound waves—can interact with the optical mode of an optical microresonator by modulation of its effective refractive index enabling optomechanical coupling. Strong confinement of third sound modes enhances their intrinsic mechanical nonlinearity paving the way for strong phonon-phonon interactions with applications in quantum optomechanics. Here, we realize a phononic crystal cavity confining third sound modes in a superfluid helium film to length scales close to the third sound wavelength. A few-nanometer-thick superfluid film is self-assembled on top of a silicon nanobeam optical resonator. The periodic patterning of the silicon material creates a periodic modulation of the superfluid film leading to the formation of a phononic band gap. By engineering the geometry of the silicon nanobeam, the phononic band gap allows the confinement of a localized phononic mode.

DOI: 10.1103/PhysRevApplied.22.L041005

Phononic crystals are structures in which periodic modulation of a material enables the engineering of the propagation of phonons [1,2]. Because of their periodic structure, phononic crystals can slow down the propagation speed of phonons or even form acoustic band gaps—frequency bands in which propagation of phonons is forbidden. Combined with advanced micro- and nanofabrication, phononic crystals enable the realization of low-loss phononic waveguides and high-quality cavities with applications in cavity optomechanics [3,4] and for realizing extremely low-loss mechanical oscillators [5]. Controlling the propagation of phonons furthermore opens the way for engineering the thermal properties of materials [6]. Phononic crystals have been realized in a variety of materials ranging from silicon and diamond [7] to graphene [8], among many others.

In recent years, superfluid helium has attracted attention as a promising material for realizing high-quality mechanical oscillators owing to the absence of viscous damping [9]. Using acoustic phonons in bulk superfluid ^{4}He, mechanical quality factors exceeding 10^7 have been achieved [10]. Acoustic phonons in superfluid helium have been utilized in cavity optomechanics experiments to realize Brillouin scattering [11], observe quantum fluctuations of the acoustic mode [12], and measure higher-order phonon correlations [13]. In these experiments a microscopic optical cavity is filled with a bulk amount of superfluid helium. The modulation of the refractive index of the superfluid inside the cavity due to density variations caused by the acoustic mode leads to optomechanical coupling. Periodic nanostructures filled with bulk superfluid have been theoretically predicted to form phononic crystals [14]. Mechanical modes in bulk superfluid helium have promising applications in the search for dark matter [15,16].

An alternative approach is superfluid thin-film optomechanics [17]: a thin layer (typical thickness 1 to 10 nm) of superfluid helium self-assembles on the surface of an optical whispering-gallery-mode microresonator due to van der Waals forces. The film supports mechanical excitations in the form of surface waves in which the thickness of the helium film is modulated, so-called "third sound" [18]. The variations of the superfluid film thickness lead to a modulation of the effective refractive index of the optical cavity mode resulting in optomechanical coupling. Using this system, laser control of third sound excitations as well as superfluid Brillouin lasing have been demonstrated [19,20]. Furthermore, the optomechanical coupling has been utilized to study quantized vortex dynamics in the superfluid film on top of the optical resonator [21].

*Contact author: s.groeblacher@tudelft.nl

The restoring force of third sound excitations in the superfluid film is the van der Waals force between the superfluid and the solid surface: $F_{\mathrm{vdW}} = \alpha_{\mathrm{vdW}}/d_{\mathrm{He}}^4$, where α_{vdW} is the Hamaker constant characteristic of the material [22]. The van der Waals force depends nonlinearly on the helium film thickness d_{He} providing an intrinsic mechanical nonlinearity of third sound modes. It has been predicted theoretically that strong mechanical nonlinearity reaching the single-phonon level can be achieved by strongly confining the third sound mode [23]. Single-phonon mechanical nonlinearities would allow the preparation of nonclassical mechanical states [24,25] as well as realizing mechanical qubits for quantum computation [26]. Strong confinement of the third sound mode requires reducing the size of the optical resonator on which the superfluid film is deposited. To achieve confinement to length scales of the order of the wavelength, phononic crystals in superfluid thin films have been proposed [23]: by periodically patterning the substrate material, a periodic modulation of the superfluid thin film is induced, which leads to the formation of phononic band gaps that can be used to confine a phononic third sound mode to length scales of around 100 nm.

Here, we design and experimentally realize a phononic crystal cavity confining third sound modes in superfluid helium thin films on silicon nanobeam optical resonators to length scales close to the third sound wavelength of $\lambda \approx 1\,\mu$m. Phononic cavity modes couple optomechanically to the high-quality optical mode enabling homodyne measurement of the mechanical mode spectrum. We demonstrate control over the mechanical resonance frequency by varying the thickness of the helium film. Lastly, we demonstrate photothermal backaction of the optical mode on the mechanical mode resulting in linewidth broadening and narrowing depending on laser frequency.

Silicon nanobeam resonators are fabricated from a silicon-on-insulator wafer with a device layer thickness of 250 nm and coated with a 3-nm alumina layer preventing further oxidation of the silicon surface. A scanning electron microscope image of a fabricated device is shown in Fig. 1(a). The nanobeam resonator is evanescently coupled to a center waveguide through which light is coupled to the device. We embed the silicon nanobeam optical resonators in a cryogenic chamber setup mounted inside a dilution refrigerator at a temperature of $T = 10$ mK as shown in Fig. 1(b). Laser light is coupled into the coupling waveguide of the device via a lensed optical fiber. Ultrapure helium gas (99.9999% elemental purity) filled into the chamber thermalizes to the cryogenic environment and becomes superfluid. As a result of attractive van der Waals forces, the superfluid helium covers all surfaces inside the chamber with a thin film of a thickness of a few nanometers, including the silicon nanobeam resonator.

The silicon nanobeam resonator confines an optical mode at a design wavelength $\lambda = 1550$ nm. Figure 1(c) shows the reflection spectrum of the optical cavity resonance of the silicon nanobeam without superfluid helium. The superfluid helium film changes the effective refractive index of the optical cavity mode causing a red shift of the resonance frequency. By comparing the measured shift of the optical resonance frequency with results of finite-element simulations, we calibrate the thickness of the superfluid helium film as more helium gas is added into the chamber, as shown in Fig. 1(d) (see Supplemental Material [27]).

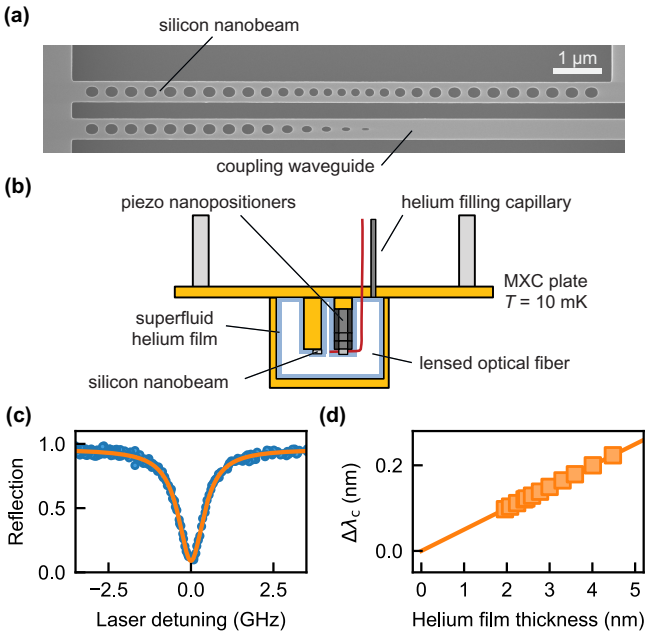

FIG. 1. Experimental setup. (a) Scanning electron microscope image of a silicon nanobeam device including coupling waveguide. (b) Schematic illustration of the cryogenic vacuum chamber setup. The chamber made from annealed copper is mounted on the mixing chamber plate of a dilution refrigerator with base temperature $T = 10$ mK and contains the silicon nanobeam sample. The chamber can be filled with helium gas through a thin stainless steel capillary. (c) Measured reflection spectrum of the optical cavity resonance without superfluid helium when scanning the laser frequency. Solid line corresponds to a Lorentzian fit with center wavelength $\lambda_c = 1551.10$ nm and linewidth $\kappa = 900$ MHz. (d) Shift of the optical resonance wavelength $\Delta\lambda_c$ as a function of helium film thickness calibrated using finite-element simulations.

The periodic patterning of the nanobeam leads to a periodic modulation of the helium film on its surface, which gives rise to a phononic band structure. We model the phononic properties of a periodically modulated superfluid film using finite-element simulations of third sound based on the approach developed in Forstner *et al.* [28]. Figures 2(a) and 2(b) show the unit cells of the helium film on the nanobeam surface for the mirror (a) and (b) center defect region. Figure 2(c) shows the resulting band structure of symmetric (red) and antisymmetric (blue) third

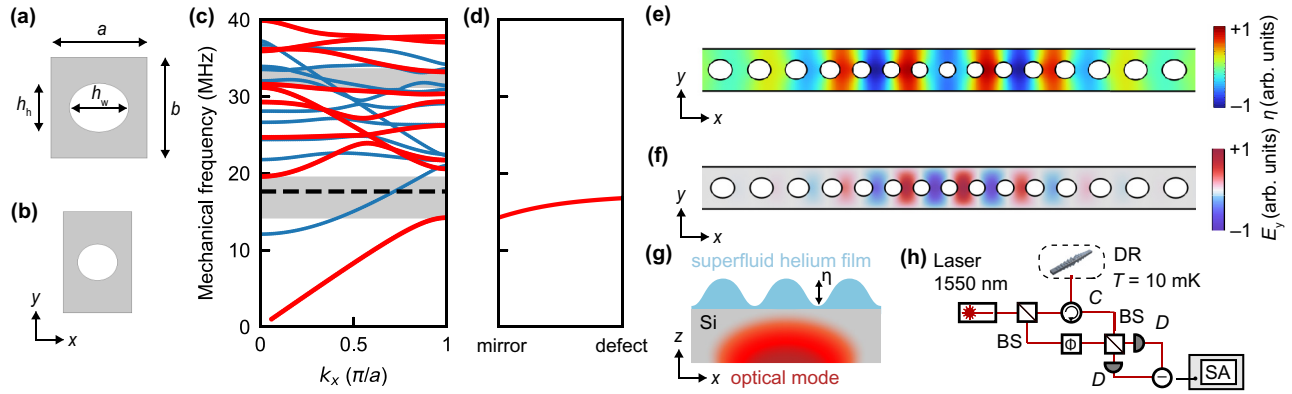

FIG. 2. Phononic crystals in thin-film superfluid helium. (a) Phononic crystal unit cell with $(a, b, h_h, h_w) = (472, 499, 241, 290)$ nm and (b) defect unit cell with $(a, b, h_h, h_w) = (332, 499, 179, 193)$ nm in superfluid helium thin film. (c) Third sound band structure of the mirror unit cell for propagation in the x direction in a helium film of thickness $d_{He} = 2.1$ nm. Symmetric (antisymmetric) modes with respect to the y direction are shown in red (blue). The phononic crystal exhibits quasiband gaps for symmetric modes for frequencies between 14 to 19 MHz and 31 to 34 MHz (gray shaded). (d) Shift of the bottom band edge at the X-point when transforming the mirror unit cell in (a) to a defect unit cell. (e) Normalized variation η of the superfluid film thickness in the mechanical mode indicated by the dashed line in (c). (f) Normalized y component of the electric field E_y in the optical cavity mode. (g) Schematic illustration of optomechanical coupling between the optical mode localized in the silicon nanobeam and a superfluid helium film with thickness variation η. (h) Optical setup for homodyne detection of third sound modes on the nanobeam. BS, beam splitter; C, circulator; D, photodiode; SA, spectrum analyzer; DR, dilution refrigerator.

sound modes in a helium film of thickness $d_{He} = 2.1$ nm for propagation in the x direction. In the following, we focus the discussion on x-symmetric modes only, as antisymmetric modes do not couple to the symmetric optical mode due to a vanishing mode overlap. The band structure exhibits quasiband gaps for symmetric modes between 14 to 19 MHz and 31 to 34 MHz. When changing the parameters of the unit cell from the mirror geometry in (a) to the defect geometry in (b) [see Fig. 2(d)], the bottom edge of the quasiband gap is continuously shifted into the band gap confining the phononic mode in the defect region. The mode profile of the confined third sound mode is shown in Fig. 2(e).

Figure 2(f) shows the distribution of the electromagnetic field in the fundamental optical mode of the silicon nanobeam. Third sound modes with surface wave amplitude η on the nanobeam surfaces modulate the refractive index around the optical cavity mode as schematically illustrated in Fig. 2(g) and therefore lead to optomechanical coupling. The optomechanical interaction transduces thermal motion of third sound modes onto the optical phase quadrature, which we read out using balanced homodyne detection [see Fig. 2(h) for a simplified sketch of the measurement setup].

We measure the mechanical spectrum of helium third sound modes by locking the laser on the optical cavity resonance and using the homodyne detection setup to detect any phase modulation of the light field. Before the superfluid film is deposited on the nanobeam resonator, no mechanical modes are visible in the spectrum between 15 and 40 MHz [cf. Fig. 3(a), orange line]. For a helium film with a thickness of $d_{He} = 2.1$ nm, the measured mechanical spectrum (blue line) shows three distinct peaks, which we can associate with third sound modes of the helium thin film: the lowest-frequency mode is the fundamental mechanical mode of the phononic crystal cavity shown in Fig. 2(e). The two peaks at higher frequencies are related to higher-order phononic modes of the superfluid film on the nanobeam geometry, which are confined by higher-order quasiband gaps in the superfluid band structure shown in Fig. 2(c). However, due to the complex band structure at higher mechanical frequencies [see Fig. 2(a)] combined with fabrication-induced imperfections of the geometry, these two peaks cannot be unambiguously identified with a specific mode shape from finite-element method (FEM) simulations. We show several of these modes and their simulated frequencies in the Supplemental Material [27]. In addition, higher-order modes in the mechanical spectrum can only be observed at the lowest helium film thicknesses. This is likely due to modifications of the quasiband gap or increased coupling to bulk phonon modes for thicker helium films inducing additional dissipation channels. We note that the superfluid phononic crystal modes on the top and bottom surface of the silicon nanobeam remain fully degenerate in frequency within the mechanical linewidth.

We measure the mechanical spectrum as a function of helium film thickness by subsequently adding more helium gas into the chamber. As shown in Fig. 3(b), the mode frequency of all observed modes in the superfluid film decreases rapidly with increasing film thickness. The restoring force for third sound modes is the van der

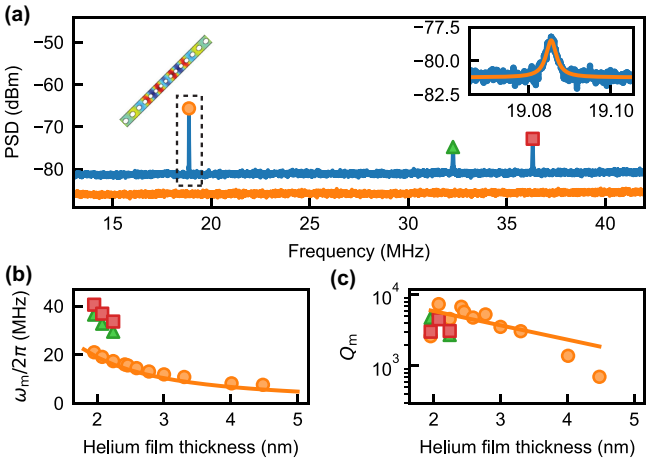

FIG. 3. Characterization of phononic crystal cavity modes in superfluid helium thin films. (a) Noise power spectral density (PSD) of third sound modes in a superfluid helium film of thickness $d_{He} = 2.1$ nm (blue) at 1.6 nW injected laser power. The inset shows an enlargement of the fundamental phononic mode indicated by the dashed box at frequency $\omega_m/2\pi = 19.085$ MHz. For reference, the spectrum recorded with 20-nW laser power without superfluid helium film is shown (orange) offset by −5 dBm for clarity. (b) Mechanical frequency and (c) quality factor of three confined third sound modes as a function of helium film thickness. Solid line in (b) corresponds to results of finite-element simulations and in (c) to a fit using an empirical expression $Q_m = a \exp(-d_{He}/l)$ with $a = (1.5 \pm 0.8) \times 10^4$ and $l = 2.2 \pm 1.0$ nm. Error bars in (b),(c) are not visible as they are smaller than the datapoint size.

Waals force between the superfluid film and the substrate, which decreases with increasing film thickness as $F_{vdW} = \alpha_{vdW}/d_{He}^4$, where α_{vdW} is the Hamaker constant characteristic of the substrate [22]. For thicker superfluid helium films, the decrease leads to spring softening and thus to a decrease in mechanical frequency. We perform finite-element simulations of the fundamental third sound mode varying the superfluid film thickness. We fit the model to the measured data with only the Hamaker constant as a free parameter and find good agreement for $\alpha_{vdW} = 0.9 \times 10^{-24}$ m^5 s^{-2}. To the best of our knowledge, this is the first time that the Hamaker constant between aluminum oxide and superfluid helium has been measured. Our approach allows one to obtain the constant for several different materials in a relatively straightforward way. We note that there is a thin (0.5-nm) layer of nitrogen ice covering the surface of the nanobeam due to imperfect vacuum during cooldown, which might impact the exact numerical value of the Hamaker constant obtained here.

Figure 3(c) shows the mechanical quality factor of both the fundamental phononic crystal cavity mode as well as the higher-order modes in the mechanical spectrum. The highest quality factor $Q_m = 7400$ is observed for the fundamental phononic mode at a film thickness $d_{He} = 2.1$ nm, while the quality factors of the higher-order modes are comparable to that of the fundamental mode. The observed mechanical quality factors are significantly higher than those of extended mechanical modes ($Q_m \approx 10^2$) that are not confined by the phononic crystal band gap (see Supplemental Material [27]).

For increasing film thickness, the mechanical quality factor decreases strongly. As discussed in Sfendla *et al.* [23], damping mechanisms intrinsic to third sound modes including pinning of quantized vortices, thermal dissipation, and breakdown of superfluidity at high flow velocities are not expected to significantly limit the attainable mechanical quality factor for the thin-film thickness and low temperatures used in this work. Instead, the mechanical quality factor in our system is likely limited by the imperfect mechanical band gap for antisymmetric modes [see Fig. 2(c)]. In the presence of geometric imperfection due to fabrication-induced disorder, coupling of the confined phononic modes to nonconfined antisymmetric modes gives rise to a mechanical dissipation channel analogous to that of conventional silicon nanobeam optomechanical crystals [5].

We now characterize the coupling between the optical and helium third sound modes by measuring the modification of the mechanical linewidth through dynamical backaction. Figure 4 shows the change in mechanical linewidth $\delta\Gamma$ for [Fig. 4(a)] the fundamental phononic crystal cavity mode and [Fig. 4(b)] the first higher-order mode in the mechanical spectrum as a function of laser detuning from the optical cavity resonance. Remarkably, for the fundamental phononic mode in Fig. 4(a) the mechanical linewidth decreases (increases) when the laser is red-detuned (blue-detuned) from the optical cavity resonance, whereas the higher-order phononic mode exhibits the opposite dependence. Such opposing signs of dynamical backaction between different mechanical modes cannot be explained through only radiation pressure coupling. Similar observations were made for microlevers in atomic force microscopy [29], as well as for third sound modes on the surface of whispering-gallery-mode resonators [19] and explained through photothermal coupling: the optical mode creates a hot spot in the center of the silicon nanobeam, which induces flow of the superfluid through the superfluid fountain effect [30]. The sign of the photothermal coupling constant σ depends on the overlap between the superfluid flow field and the respective third sound mode and can thus vary between modes. For opposing signs of the photothermal coupling constant, the dependence of mechanical linewidth on laser detuning can be fitted using an analytical model (see Supplemental Material [27]), as shown by solid lines in Fig. 4. The model characterizes the photothermal coupling with time constant τ through an effective coupling parameter $G_{eff} = G\sqrt{\tau/(1+\omega_m^2\tau^2)}$. The coupling constant $G = g_0\gamma_{pt}$ contains the radiation pressure coupling rate g_0 and the ratio between photothermal and radiation pressure force γ_{pt}.

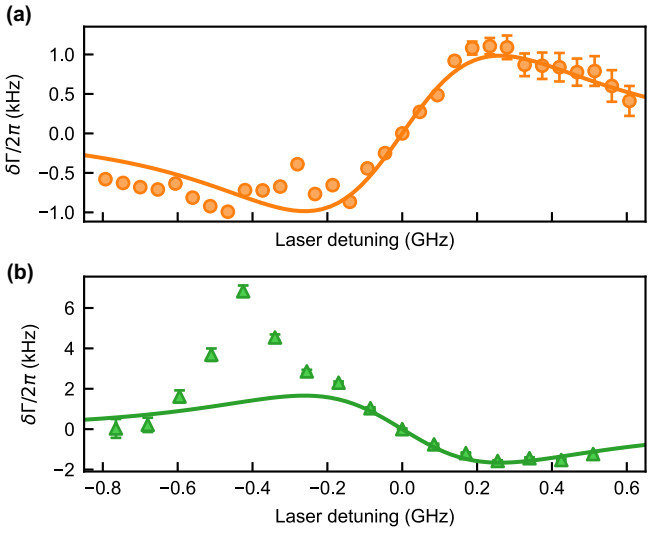

FIG. 4. Photothermal backaction on helium phononic crystal cavity modes. Shift of the mechanical linewidth $\delta\Gamma$ as a function of laser detuning for (a) the fundamental and (b) the first higher-order mechanical mode for helium film thickness $d_{\mathrm{He}} = 2.2\,\mathrm{nm}$. When the laser is on resonance with the optical cavity, these modes have mechanical linewidths of $\Gamma_{\mathrm{m},1} = 2.7\,\mathrm{kHz}$ and $\Gamma_{\mathrm{m},2} = 8.2\,\mathrm{kHz}$ and mechanical frequencies $\omega_{\mathrm{m},1}/2\pi = 17.3\,\mathrm{MHz}$ and $\omega_{\mathrm{m},2}/2\pi = 29.4\,\mathrm{MHz}$, respectively. Solid lines correspond to fits obtained from photothermal theory (see Supplemental Material [27]). The sign of the photothermal coupling constant σ is negative (positive) for the fundamental (first higher-order) mode.

We report effective coupling parameters of $G_{\mathrm{eff},1}/2\pi = 2.1\,\mathrm{Hz}\sqrt{\mathrm{s}}$ and $G_{\mathrm{eff},2}/2\pi = 1.8\,\mathrm{Hz}\sqrt{\mathrm{s}}$ for the fundamental and first higher-order phononic modes, respectively. As discussed in the Supplemental Material [27], we estimate the value of the photothermal time constant $\tau = 3.7\,\mu\mathrm{s}$ allowing us to obtain the coupling constants $G_1/2\pi = 430\,\mathrm{kHz}$ and $G_2/2\pi = 650\,\mathrm{kHz}$. From FEM simulations, we further estimate $g_0/2\pi = 20\,\mathrm{kHz}$ for the fundamental phononic crystal cavity mode. This allows us to estimate the ratio of photothermal to radiation pressure coupling to be $\gamma_{\mathrm{pt}} = 21.5$. We observe a large mechanical linewidth of the higher-order mode in Fig. 4(b) around a laser detuning of $-0.5\,\mathrm{GHz}$. While the cause for this observation warrants further investigation in the future, we propose that it might be due to interaction of the third sound mode with quantized vortices [21]. The photothermal interaction is also theoretically expected to lead to a change in mechanical frequency as a function of laser detuning. However, the observation of this shift in our experiment is obscured by a frequency shift due to laser heating of the helium film likely originating from absorption heating of the silicon substrate [31,32] (see Supplemental Material [27]).

In conclusion, we have designed and experimentally demonstrated a phononic crystal cavity for third sound modes in a superfluid helium thin film on a silicon nanobeam optical resonator. Confined phononic modes with mechanical quality factors up to $Q_{\mathrm{m}} = 7400$ are observed through their optomechanical interaction with the optical mode of the silicon nanobeam. The mechanical mode frequency decreases with increasing helium film thickness in good agreement with finite-element simulations. The optomechanical interaction causes dynamical backaction on the mechanical mode, which we find is dominated by photothermal coupling.

Previous experiments in superfluid thin-film optomechanics were based on superfluid films assembled on whispering-gallery-mode optical microresonators with diameters of the order of 50 to 100 μm [19–21]. The phononic crystal cavity presented in this work reduces this confinement length by almost 2 orders of magnitude to about 5 μm for the fundamental phononic crystal cavity mode and 1 μm for select higher-order modes (see Supplemental Material [27]), bringing superfluid third sound modes close to the regime of strong mechanical nonlinearity, where the single-phonon nonlinear frequency shift of the mechanical mode $\delta\omega_{\mathrm{m}}$ is larger than the mechanical linewidth Γ_{m}. Based on finite-element simulations, we estimate $\delta\omega_{\mathrm{m}}/2\pi = 7\,\mathrm{mHz}$ for the fundamental phononic crystal cavity mode and $\delta\omega_{\mathrm{m}}/2\pi = 88\,\mathrm{mHz}$ for the higher-order mode with shortest confinement length (see Supplemental Material [27]). Reaching the single-phonon nonlinear regime requires both stronger confinement of the phononic mode to an even smaller mode volume as well as an increased mechanical quality factor. A modest increase of the mechanical confinement to defect sizes of the order of 100 nm and an increased mechanical quality factor of around $Q_{\mathrm{m}} = 10^6$ will enable nonlinearities on the single-phonon level [23]. Both should be within reach by designing phononic crystal structures that are optimized for third sound modes and not for optomechanical operation. In particular, reducing phonon radiation loss through phononic mirrors by surrounding the nanobeam with a phononic shield with full phononic band gap similar to phononic shield structures established in silicon optomechanical crystals [5,33,34] will significantly boost the mechanical quality factor. Bringing the system close to the single-phonon nonlinear regime will first manifest in asymmetric mechanical lineshapes and eventually in the splitting of the mechanical spectrum [23]. Finally reaching the single-phonon nonlinear regime will open up approaches for creating nonclassical states of mechanical motion [24,25] and pave the way for realizing mechanical qubits for quantum computation [26].

Acknowledgments. We would like to thank Xiong Yao and Liu Chen for helpful discussions. We further acknowledge assistance from the Kavli Nanolab Delft. This work is financially supported by the European Research Council (ERC CoG Q-ECHOS, 101001005) and is part of the research program of the Netherlands Organization

for Scientific Research (NWO), supported by the NWO Frontiers of Nanoscience program, as well as through a Vrij Programma (680-92-18-04) grant.

[1] M. M. Sigalas, and E.N. Economou, Elastic and acoustic wave band structure, J. Sound Vib. **158**, 377 (1992).

[2] M. S. Kushwaha, P. Halevi, L. Dobrzynski, and B. Djafari-Rouhani, Acoustic band structure of periodic elastic composites, Phys. Rev. Lett. **71**, 2022 (1993).

[3] M. Eichenfield, J. Chan, R. M. Camacho, K. J. Vahala, and O. Painter, Optomechanical crystals, Nature **462**, 78 (2009).

[4] M. Aspelmeyer, T. J. Kippenberg, and F. Marquardt, Cavity optomechanics, Rev. Mod. Phys. **86**, 1391 (2014).

[5] G. S. MacCabe, H. Ren, J. Luo, J. D. Cohen, H. Zhou, A. Sipahigil, M. Mirhosseini, and O. Painter, Nano-acoustic resonator with ultralong phonon lifetime, Science **370**, 840 (2020).

[6] M. Nomura, R. Anufriev, Z. Zhang, J. Maire, Y. Guo, R. Yanagisawa, and S. Volz, Review of thermal transport in phononic crystals, Mater. Today Phys. **22**, 100613 (2022).

[7] K. Kuruma, B. Pingault, C. Chia, M. Haas, G. D. Joe, D. R. Assumpcao, S. W. Ding, C. Jin, C. J. Xin, M. Yeh, N. Sinclair, and M. Lončar, Engineering phonon-qubit interactions using phononic crystals, arXiv:2310.06236.

[8] J. N. Kirchhof, K. Weinel, S. Heeg, V. Deinhart, S. Kovalchuk, K. Höflich, and K. I. Bolotin, Tunable graphene phononic crystal, Nano Lett. **21**, 2174 (2021).

[9] G. S. Agarwal and S. S. Jha, Theory of optomechanical interactions in superfluid He, Phys. Rev. A **90**, 023812 (2014).

[10] L. A. D. Lorenzo and K. C. Schwab, Superfluid optomechanics: Coupling of a superfluid to a superconducting condensate, New J. Phys. **16**, 113020 (2014).

[11] A. D. Kashkanova, A. B. Shkarin, C. D. Brown, N. E. Flowers-Jacobs, L. Childress, S. W. Hoch, L. Hohmann, K. Ott, J. Reichel, and J. G. E. Harris, Superfluid Brillouin optomechanics, Nat. Phys. **13**, 74 (2017).

[12] A. Shkarin, A. Kashkanova, C. Brown, S. Garcia, K. Ott, J. Reichel, and J. Harris, Quantum optomechanics in a liquid, Phys. Rev. Lett. **122**, 153601 (2019).

[13] Y. Patil, J. Yu, S. Frazier, Y. Wang, K. Johnson, J. Fox, J. Reichel, and J. Harris, Measuring high-order phonon correlations in an optomechanical resonator, Phys. Rev. Lett. **128**, 183601 (2022).

[14] S. Spence, Z. Koong, S. Horsley, and X. Rojas, Superfluid optomechanics with phononic nanostructures, Phys. Rev. Appl. **15**, 034090 (2021).

[15] C. G. Baker, W. P. Bowen, P. Cox, M. J. Dolan, M. Goryachev, and G. Harris, Optomechanical dark matter instrument for direct detection, Phys. Rev. D **110**, 043005 (2024).

[16] M. Hirschel, V. Vadakkumbatt, N. P. Baker, F. M. Schweizer, J. C. Sankey, S. Singh, and J. P. Davis, Superfluid helium ultralight dark matter detector, Phys. Rev. D **109**, 095011 (2024).

[17] C. G. Baker, G. I. Harris, D. L. McAuslan, Y. Sachkou, X. He, and W. P. Bowen, Theoretical framework for thin film superfluid optomechanics: Towards the quantum regime, New J. Phys. **18**, 123025 (2016).

[18] K. R. Atkins, Third and fourth sound in liquid helium II, Phys. Rev. **113**, 962 (1959).

[19] G. I. Harris, D. L. McAuslan, E. Sheridan, Y. Sachkou, C. Baker, and W. P. Bowen, Laser cooling and control of excitations in superfluid helium, Nat. Phys. **12**, 788 (2016).

[20] X. He, G. I. Harris, C. G. Baker, A. Sawadsky, Y. L. Sfendla, Y. P. Sachkou, S. Forstner, and W. P. Bowen, Strong optical coupling through superfluid Brillouin lasing, Nat. Phys. **16**, 417 (2020).

[21] Y. P. Sachkou, C. G. Baker, G. I. Harris, O. R. Stockdale, S. Forstner, M. T. Reeves, X. He, D. L. McAuslan, A. S. Bradley, M. J. Davis, and W. P. Bowen, Coherent vortex dynamics in a strongly interacting superfluid on a silicon chip, Science **366**, 1480 (2019).

[22] C. Enss and S. Hunklinger, *Low-Temperature Physics* (Springer Science & Business Media, Berlin, 2005).

[23] Y. L. Sfendla, C. G. Baker, G. I. Harris, L. Tian, R. A. Harrison, and W. P. Bowen, Extreme quantum nonlinearity in superfluid thin-film surface waves, npj Quantum Inf. **7**, 1 (2021).

[24] S. Rips, M. Kiffner, I. Wilson-Rae, and M. J. Hartmann, Steady-state negative Wigner functions of nonlinear nanomechanical oscillators, New J. Phys. **14**, 023042 (2012).

[25] S. Rips, I. Wilson-Rae, and M. J. Hartmann, Nonlinear nanomechanical resonators for quantum optoelectromechanics, Phys. Rev. A **89**, 013854 (2014).

[26] S. Rips and M. J. Hartmann, Quantum information processing with nanomechanical qubits, Phys. Rev. Lett. **110**, 120503 (2013).

[27] See Supplemental Material at http://link.aps.org/supplemental/10.1103/PhysRevApplied.22.L041005 for additional experimental details and theoretical modeling.

[28] S. Forstner, Y. Sachkou, M. Woolley, G. I. Harris, X. He, W. P. Bowen, and C. G. Baker, Modelling of vorticity, sound and their interaction in two-dimensional superfluids, New J. Phys. **21**, 053029 (2019).

[29] G. Jourdan, F. Comin, and J. Chevrier, Mechanical mode dependence of bolometric backaction in an atomic force microscopy microlever, Phys. Rev. Lett. **101**, 133904 (2008).

[30] J. F. Allen and H. Jones, New phenomena connected with heat flow in helium II, Nature **141**, 243 (1938).

[31] S. M. Meenehan, J. D. Cohen, S. Gröblacher, J. T. Hill, A. H. Safavi-Naeini, M. Aspelmeyer, and O. Painter, Silicon optomechanical crystal resonator at millikelvin temperatures, Phys. Rev. A **90**, 011803 (2014).

[32] S. M. Meenehan, J. D. Cohen, G. S. MacCabe, F. Marsili, M. D. Shaw, and O. Painter, Pulsed excitation dynamics of an optomechanical crystal resonator near its quantum ground state of motion, Phys. Rev. X **5**, 041002 (2015).

[33] J. Chan, A. H. Safavi-Naeini, J. T. Hill, S. Meenehan, and O. Painter, Optimized optomechanical crystal cavity with acoustic radiation shield, Appl. Phys. Lett. **101**, 081115 (2012).

[34] A. Wallucks, I. Marinković, B. Hensen, R. Stockill, and S. Gröblacher, A quantum memory at telecom wavelengths, Nat. Phys. **16**, 772 (2020).